Finite Difference Analysis of 2-D Photonic Crystals

Hung Yu David Yang, *Senior Member, IEEE*

Abstract— **In this paper, a finite difference method is developed to analyze the guided-wave properties of a class of two-dimensional photonic crystals (irregular dielectric rods). An efficient numerical scheme is developed to deal with the deterministic equations resulting from a set of finite difference equations for inhomogeneous periodic structures. Photonic band structures within an irreducible Brillouin zone are investigated for both in-plane and out-of-plane propagation. For out-of-plane propagation, the guided waves are hybrid modes; while for in-plane propagation, the guided waves are either TE or TM modes, and there exist photonic bandgaps within which wave propagation is prohibited. Photonic bandgap maps for squares, veins, and crosses are investigated to determine the effects of the filling factor, the dielectric contrast, and lattice constants, on the band-gap width and location. Possible applications of photonic bandgap materials are discussed.**

I. Introduction

In recent years, there has been growing research activities related to the development of artificial electrical or optical materials. By tailoring the material electrical characteristics, one is able to control the flow of electromagnetic waves from microwave to optical frequencies. Wave propagation in periodic structures has been an important subject in microwaves and optics for many decades. Artificial dielectrics composed of infinite arrays of periodic conductors have been proposed for microwave lens applications [1]. Periodically loaded waveguides have found applications in a variety of devices such as traveling-wave tubes, filter networks, and surface waveguiding devices [2]. Planar printed metallic elements periodically distributed over the surface of a dielectric layer has been used in frequency selective surfaces [3] and integrated phased array antennas [4]. Light interaction with dust and rain drops and X-ray diffraction from crystals are examples of wave interaction with randomly distributed periodic structures [5]. A common feature of periodic structures is the existence of frequency bands where electromagnetic waves are highly attenuating and do not propagate. In analogy to an electrical crystal where periodic atoms or molecules may present a bandgap prohibiting electron propagation, a photonic crystal is made of macroscopic dielectrics periodically placed (or embedded) within surrounding media. The periodic nature of the structure may introduce photonic bandgap (PBG) within which photons (waves) are forbidden in certain directions.

Artificial materials made of periodic dielectrics exhibiting a complete photonic bandgap (PBG) have been proposed to prevent spontaneous emission in semiconductor lasers and heterojunction bipolar transistors [7]. There is tremendous potential in various electronic and optical applications. The consensus is that optical and electromagnetic technologies may benefit from photonic crystals in a similar way electronic technology benefits from semiconductors.

Electromagnetic modeling plays an important role in the design and applications of artificial materials. Field analysis and simulation are indispensable for material and component development. Electromagnetic wave theory and computational techniques are necessary to determine the fundamental physical principles of material properties and the design of devices and components from microwave to optical frequencies. A plane-wave-expansion method has been extensively used for the analysis of two-dimensional (2-D) and three-dimensional (3-D) photonic bandgap materials [8]–[9]. In this method, the eigenvalues (frequencies) and eigenvectors (magnetic fields) are found iteratively from a large dense matrix (matrix dimension is twice of the number of plane wave terms).

In this paper, an efficient finite difference method is developed for the photonic band structures of a class of 2-D photonic crystals. There are several advantages of the finite difference method over the plane wave methods. The characteristic matrix in the finite difference method is sparse (quasi-band diagonal) and only nonzero elements need to be stored. An efficient numerical scheme with direct QR procedures utilizing the matrix sparsity is developed to reduce the computation time significantly. In addition, all the eigenvalues can be found from a direct root search routine (bisection method) avoiding the initial guess for each eigenvector needed in the iterative methods. The finite difference method is appropriate for computer aided design of the photonic crystals. A limitation of finite difference method is that the crystal "atoms" are particularly suitable for irregular, but not curved shapes.

The photonic crystal structure can be made with conventional machine tools in the centimeter range and with micromachining techniques in the micron range. For 2-D photonic crystals, the in-plane propagation is of particular interest due to the existence of a photonic bandgap where wave propagation is prohibited in all directions. For some applications, we need to understand the guided-wave characteristics in an arbitrary direction. The analysis for both in-plane and out-of-plane propagation are considered in this paper. The finite difference results are compared in special cases with those with an integral-equation method and a plane-wave-expansion method to confirm the validity of the presented results.

II. Finite Difference Analysis of 2-D Periodic Structures

For 2-D photonic crystals, the geometry is uniform along the longitudinal ($\hat{z}$) direction and periodic in the transverse (in-plane) directions with lattice constants a and b. The cross

Manuscript received March 28, 1996.

The author is with the Department of Electrical Engineering and Computer Science, University of Illinois at Chicago, IL 60607 USA.

Publisher Item Identifier S 0018-9480(96)08537-7.

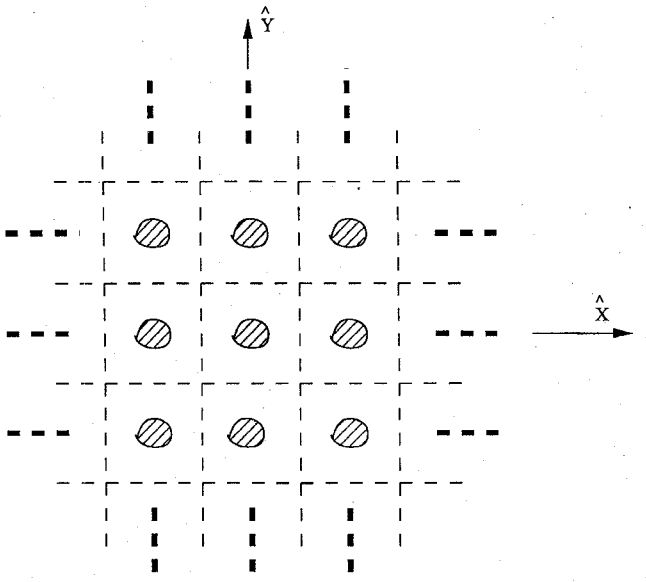

Fig. 1. Cross section of a two dimensional photonic crystal: Periodic arrays of dielectric rods in a homogeneous dielectric medium.

section of a general two-dimensional photonic crystal is shown in Fig. 1. The geometry is somewhat similar to periodic arrays of dielectric waveguides.

A finite difference method for periodic structures is used for the computation of the propagation constant of guided wave propagating in an arbitrary direction. For hybrid mode analysis of waveguide structures (out-of-plane propagation), we use Helmholtz equations with two field components. In finite element or finite difference method, an H-field formulation is more preferable due to the fact that magnetic field is continuous. In this analysis, the H_x and H_y formulation is employed to avoid possible spurious-mode problems [10], although any of the two magnetic-field components can be used. The Helmholtz equations of the pertinent problem are

$$\frac{\partial^2 H_x^{(i)}}{\partial x^2} + \frac{\partial^2 H_x^{(i)}}{\partial y^2} + \left(k_i^2 - \beta z^2\right) H_x^{(i)} = 0 \tag{1}$$

and

$$\frac{\partial^2 H_y^{(i)}}{\partial x^2} + \frac{\partial^2 H_y^{(i)}}{\partial y^2} + \left(k_i^2 - \beta_z^2\right) H_y^{(i)} = 0 \tag{2}$$

where β_z is the phase constant in the $\hat{z}$ direction, $k_i = k_0\sqrt{\varepsilon_i}$ with k_0 the free-space wave number, and ε_i is the dielectric constant in region i. In finite difference method, the unit cell $0 \le x \le a$ and $0 \le y \le b$ is divided into many rectangular grids. A unit cell for periodic dielectric crosses with the finite difference mesh is illustrated in Fig. 2. The common point of four adjacent grids is a central node where H_x and H_y are related to those of the adjacent nodes through a five-point finite difference equation. Five-point finite difference equations of the transverse magnetic fields for four connected grids with different dielectric constants have been derived in [10], and the results are shown in the Appendix. For the periodic structures, if there are $M+1$ nodes in each side of a unit cell, there are $2M^2$ finite difference equations with $2M^2$ unknowns. For the central nodes at the boundary, some of the adjacent nodes are out of the unit cell and can be brought back into the unit cell

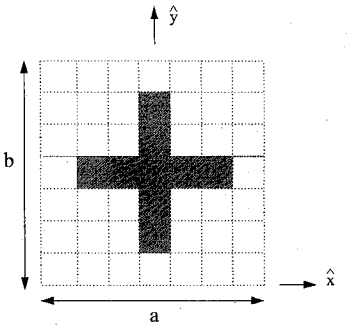

Fig. 2. A unit cell of periodic dielectric crosses and finite difference meshes.

through the periodic boundary conditions,

$$\Phi(x+a, y+b) = e^{-j\beta_x a - j\beta_y b}\Phi(x,y). \tag{3}$$

Here $\Phi(x,y)$ is any field component, β_x and β_y and are the phase constants in the $\hat{x}$ and $\hat{y}$ directions, respectively. Also, due to the periodic property, the nodes at only two of the four cell boundaries are included in the matrix equations. The $2M^2$ finite difference equations are a set of linear homogeneous equations, which can be written in a matrix form as

$$\left\{[A] - \left(\frac{\omega}{c}\right)^2 [I]\right\}[H] = 0. \tag{4}$$

$[H]$ is a column matrix, where the elements are the transverse magnetic fields at the central nodes. $[I]$ is the identity matrix. $[A]$ is the characteristic matrix and is a function of the phase constants and the geometric and material parameters. The eigenvalues $(\omega/c)^2$ are the square of the free-space wave number. There are $2M^2$ eigenvalues in (4). For the photonic band structure of interest, we need to find the first few eigenvalues (usually the first six). The eigenvalue equation is obtained by setting the matrix determinant to zero. The roots of the eigenvalue equation are the frequencies, for a given set of the phase constants.

In numerical implementation, direct approach using Gaussian elimination to find the matrix determinant is not practical. The bisection method of root searching (zeros of the matrix determinant) often requires many iterations, especially for photonic band structures. For a unit cell with 400 grids (20 divisions in each direction), the matrix dimension would be 800. The required computer memory and time for root searching would be enormous. A careful examination of the characteristic matrix $[A]$ shows that most of the matrix elements are zero. This is not surprising, since each row is obtained from a five-point finite difference equation and has at most nine nonzero elements. The distribution of zeros within the matrix $[A]$ is shown in Fig. 3(a). All the nonzero elements are within the gray area. In finite difference method for a bounded region, the matrix is completely band-diagonal. There are available standard software packages such as EISPACK [11] to find the eigenvalues of such a banded matrix. For the pertinent periodic problem, It is seen that the matrix is band-diagonal except some nonzeros at the end of the first few rows and columns (quasi-band-diagonal). Those nonzeros off the diagonal band are due to the central nodes at the boundary of a unit cell. The existing software packages do not facilitate

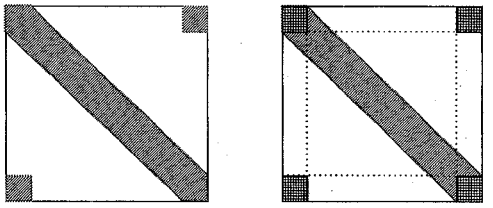

(a) (b)

Fig. 3. Quasi-banded matrix due to a 2-D finite difference analysis of 2-D periodic structures. Note that nonzero elements are in the gray area.

efficient evaluation of eigenvalues for such a quasi-banded matrix. In this work, a numerical scheme is developed for such a quasi-banded matrix.

For the convenience of discussion, we assume that there are $M+1$ nodes on each side of a unit cell, and there are $2M^2$ finite difference equations. The purpose of the algorithm is to evaluate the determinant of the eigenvalue matrix in (4). It can be shown that the maximum dimension for a square submatrix within the gray strip in Fig. 3(a) is $2(M+1)$. For the moment, we assume that all the off-band diagonal terms are all zero so that we are dealing with a banded matrix. In this case we would need to deal with a square matrix with dimension $2(M+1)$, not the entire matrix. In order to show how this works, we start from the square submatrix at the very left of the gray strip in Fig. 3(a). In a QR procedure, we apply Gaussian elimination $2M+1$ times to obtain the first diagonal term of the final tri-diagonal matrix (the multiplication of all diagonal terms is the determinant we are looking for), and we then eliminate the first row and column. The important feature of this procedure is that all the operations are within the gray strip and the resulting one-dimension-less matrix is still banded. We may repeat this procedure until only the last (the one at the very right side) square submatrix is left. We then use a standard QR procedure to find the determinant of this last submatrix. The advantage of this approach is that all the matrices involved are with a dimension $2(M+1)$ instead of $2M^2$, and Gaussian elimination is for elements within the band. This approach reduces the computer time and memory tremendously (about the square root of the computer time with the direct QR procedure). We will extend this algorithm to deal with the quasi-band-diagonal matrix shown in Fig. 3(a).

It can be shown that the submatrices off the diagonal band in Fig. 3(a) are square matrices with a dimension $2M$. In order to deal with these submatrices, we divide the matrix in Fig. 3(a) into several subregions as shown in Fig. 3(b). It is interesting to see that if we exclude the four submatrices in the four corners, the rest of the whole matrix is band-diagonal. It is even more interesting to note that if we apply Gaussian elimination to the band-diagonal part, the four excluded submatrices are unaffected. If we begin the row and column elimination, the band-diagonal part of the matrix starts to shrink until the four excluded submatrices merge into one matrix with dimension $4M$. The determinant of the remaining matrix is solved by a standard QR procedure.

The proposed numerical scheme utilizing the matrix sparsity reduces significantly the computer time and memory compared to a direct approach. For a typical case of a square unit cell with 400 grids, the proposed scheme involves with a matrix with dimension 80 instead of 800. This results in reducing computer memory by a factor of 100. The computer time reduction is more than 100 times.

TABLE I

No. of Nodes ($M \times N$)	First Mode β/k_0	Second Mode β/k_0
36 ($M=N=6$)	2.5977	2.3173
121 ($M=N=11$)	2.5438	2.3204
256 ($M=N=16$)	2.5258	2.3292
441 ($M=N=21$)	2.5172	2.3345

TABLE II

No. of Nodes ($M \times N$)	First Mode β/k_0	Second Mode β/k_0
36 ($M=N=6$)	1.8813	1.8528
100 ($M=N=10$)	1.9375	1.9073
196 ($M=N=14$)	1.9516	1.9204
324 ($M=N=18$)	1.9568	1.9249
428 ($M=N=22$)	1.9591	1.9268

The discussion so far is for general out-of-plane propagation, where the waves are hybrid. For in-plane propagation ($\beta_z = 0$), the guided waves are either TE or TM (to z) modes. For TE modes, only H_z, E_x, and E_y components exist. For TM modes, only E_z, H_x, and H_y components exist. Five-point finite difference equations for TE and TM modes are in terms of H_z and E_z, respectively. These two equations are shown in the Appendix. For in-plane propagation, the characteristic matrix is in the same form as shown in Fig. 3(a). However, the number of equations and unknowns are half of the those for out-of-plane propagation. The numerical algorithms for both cases are the same.

III. Results and Discussions

The finite difference method can deal with a variety of irregular photonic crystal structures. The cross section of unit cells of several photonic crystals investigated in this paper is shown in Fig. 4. Convergence tests are performed for two cases shown in Tables I and II. Both cases are for out-of-plane propagation. The first case is for air crosses within a dielectric medium. The second case is for air squares within a dielectric medium. It is seen that the results are convergent as the number of grids within a unit cell increases. Generally, 400 grids provide excellent convergent results. Computer time in a PC for the 400 grid case in Table I is about 100 seconds for each data. For in-plane propagation, computer time is about 20 seconds instead.

The validity of the finite difference results is checked by comparing with the results from an integral equation method [12]. This comparison is for the case of periodic square dielectric waveguides surrounded by air and the propagation is in the z direction (out-of-plane). The results of the comparison are shown in Fig. 5. The plot is for phase-constant versus the ratio of square-width to lattice-constant. The comparison shows excellent agreement. The finite difference results for in-plane propagation are compared with the plane-wave-

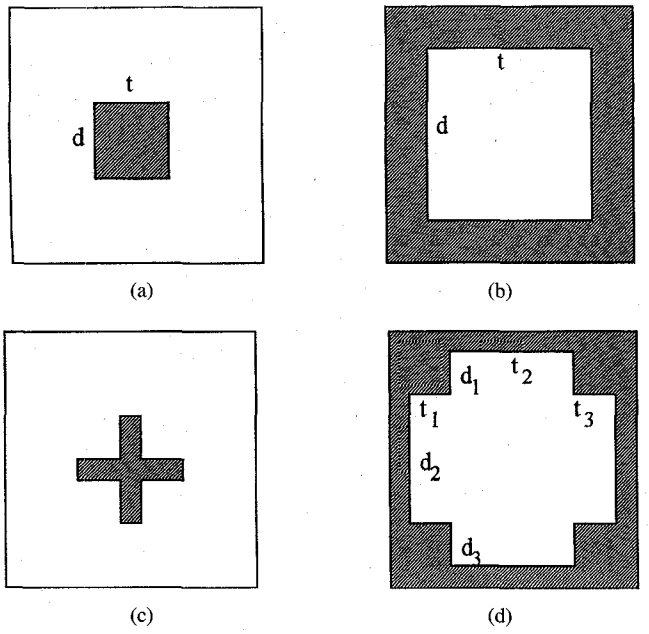

Fig. 4. Cross section of unit cells of four types of 2-D photonic crystals.

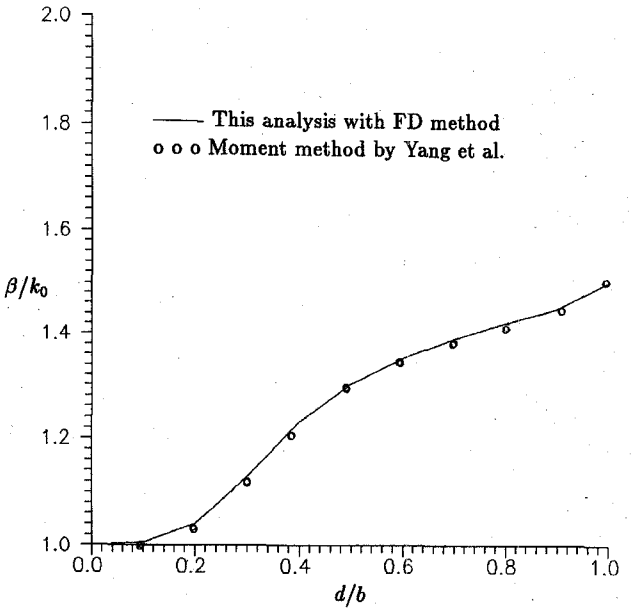

Fig. 5. Phase constant of the fundamental mode of dielectric squares surrounded by air. $F = 10$ GHz, $a = 6$ cm, $b = 3$ cm, $t = 2d$, $\varepsilon_r = 2.25$, $\hat{z}$ direction propagation.

expansion method [8]. The results of the comparison are shown in Fig. 6. The comparison is for the case of air squares in a dielectric medium (or dielectric veins in Fig. 4(b) when the size of the square is close to a unit cell). The plot is for the photonic band structure of TE modes. Excellent agreement is found between the two methods. The horizontal axis in Fig. 6 is for the phase constants of guided wave modes in various directions. Due to symmetric and periodic properties, only the shaded region in the Brillouin zone (the wave number space or the reciprocal lattice) is irreducible. For example, the phase constants in the $\hat{x}, \hat{y}, -\hat{x}$, and $-\hat{y}$ direction propagation are all the same. Also, the maximum phase constant in the $\hat{x}$ direction within the Brillouin zone is π/a. The fact that there exists a photonic bandgap where wave propagation is prohibited in all directions is of particular interest. Within the bandgap region, the modes become pairs of complex modes that do not carry power. Similar complex modes have been found in dielectric loaded waveguides [13].

Photonic band structures for periodic dielectric squares are shown in Fig. 7 for both TE and TM modes. It is seen from Fig. 7 that there exists a wide band photonic gap for TM waves (but not for TE waves). Generally, there may exist only TM photonic bandgaps for dielectric squares embedded within a lower dielectric material. In contrast, dielectric squares surrounded by a higher dielectric (dielectric veins) may have a wide bandgap for TE waves. It is found that TM photonic bandgap may also exist for dielectric veins, but the bandgap is usually narrow. A general observation is that with a proper filling factor, low dielectric materials with physically isolated high-dielectric implants show a wide TM bandgap; while low dielectric materials with connected, slim, and higher-dielectric implants show a wide TE bandgap.

Photonic band structures of slim dielectric crosses for both TE and TM modes are shown in Fig. 8. Note that if the arms of the crosses extend to the entire lattice [see Fig. 4(c)], the

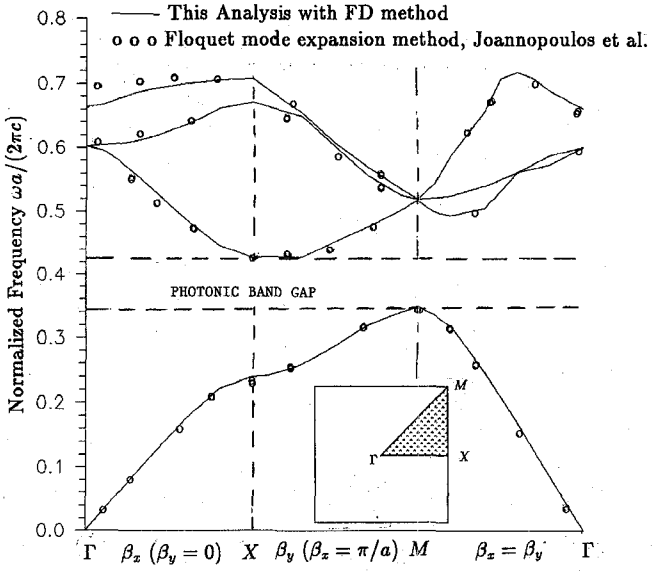

Fig. 6. The photonic band structure for the first four TE modes of square dielectric veins ($\varepsilon_r = 8.9$) in air. The horizontal axis is for wave numbers in different directions. Γ, X, M are symmetric points in Brillouin zone shown in the inset.

structure becomes a dielectric vein structure [see Fig. 4(b)]. Basically, we can treat the periodic cross structure as a periodic broken vein structure, which tends to have a TE photonic bandgap. On the other hand, dielectric crosses are isolated implants, which tend to have a TM bandgap. Therefore, there should exist both TE and TM bandgaps as are indeed observed in Fig. 8. Generally, the TE bandgap occurs at higher frequencies than the TM bandgap. The length of the cross arm may be used to adjust the bandgap width.

The photonic band structures of air crosses within a dielectric medium for both TE and TM modes are shown in Fig. 9. The cross arms for this case are relatively wide (see

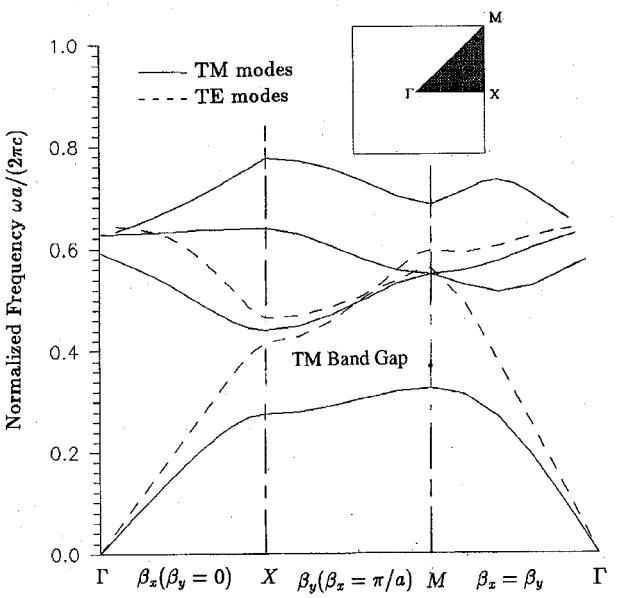

Fig. 7. The photonic band structure for the first few modes of dielectric squares $\varepsilon_r = 8.9$ surrounded by air. The square length is $0.3545a$. The horizontal axis is for wave numbers in different directions. Γ, X, M are symmetric points in Brillouin zone shown in the inset.

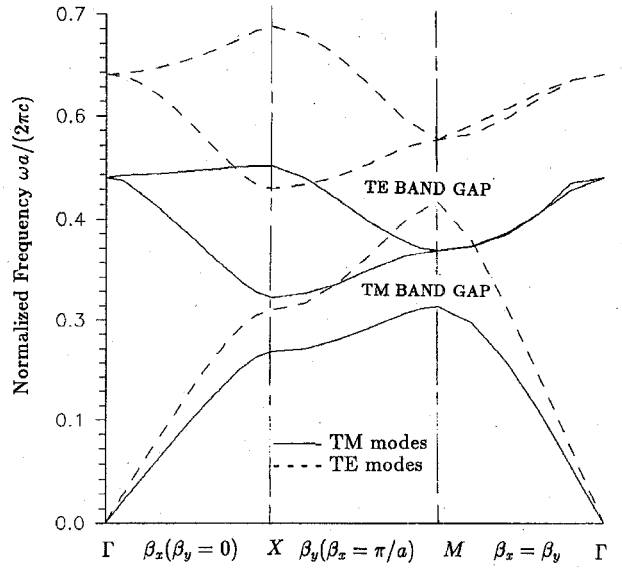

Fig. 8. The photonic band structure for the first few modes of dielectric crosses. Dielectrics ε_r=8.9 is surrounded by air. $t_1 = t_2 = d_1 = d_2 = 0.3445a$ and $t_2 = d_2 = 0.181a$.

Fig. 4(d)), and the geometry is equivalently a dielectric vein structure with additional dielectric at the junctions of the veins. The dielectric addition may be used to control the TE and TM bandgap width. Its effect is to increase the TM bandgap width and reduce the TE bandgap width. In the extreme case when the air crosses are slim, both TE and TM bandgaps vanish.

The frequencies and band width of photonic bandgap in 2-D photonic crystals are determined by the crystal geometry, lattice constant, the filling factor, and the dielectric contrast. For a given implant shape, the filling factor and the dielectric constant ratio determine the photonic band characteristics. Other parameters are scalable. Photonic bandgap maps

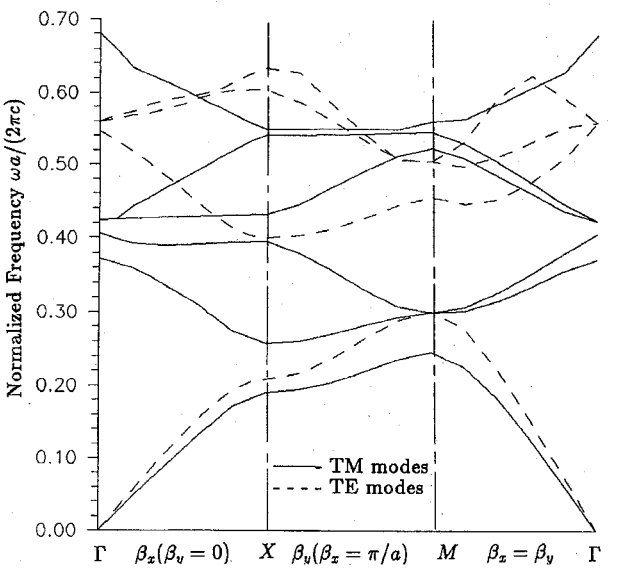

Fig. 9. The photonic band structure for the first few modes of air crosses within a dielectric $\varepsilon_r = 12$ medium. $t_1 = t_3 = d_1 = d_3 = 0.091a$ and $t_2 = d_2 = 0.7a$.

(bandgap zones versus filling factor) for dielectric square and vein structures, which are useful for the design, are shown in Fig. 10. The dielectric constant of the material is 11 and the surrounding medium is air. For TM modes of dielectric squares, it is observed that the bandgap exists when the filling factor $(t/b)^2$ is in between 0.03 to 0.55. The boundary frequencies of the gap decrease as the filling factor increases, and the widest bandgap occurs when the filling factor is about 0.1. A TE bandgap is not found for the dielectric squares within air. It is observed from Fig. 10 that the TE and TM bandgap may both exist for dielectric veins in the air. The TE bandgap exists for a wide range of filling factor, from 0.25 to 0.86. The widest bandgap occurs when the filling factor is about 0.7 and the boundary frequencies of the gap increase as the filling factor increases. The corresponding TM bandgap occurs at much smaller range of filling factor (0.6 to 0.85), and the bandwidth is much smaller.

The bandgap maps for symmetric dielectric crosses in air are shown in Fig. 11. The structure can be treated as broken dielectric veins. The bandgap frequencies are plot against the air gap length (air gap length is $2x$). When the air gap is zero and the veins are all connected, we observe a wide TE bandgap and no TM bandgap (see Fig. 6). When the veins are broken with air gap and the air gap increases, the TE bandgap quickly decreases to zero and TM bandgap width starts to increase (all the crosses become isolated). It has been found that circular air columns in a triangle lattice exhibit TE and TM bandgap overlap [8]. A similar observation is not found for rectangular air columns in a triangle lattice or any other structures presented in this paper.

For practical purposes, we need to understand the wave propagation in an arbitrary direction ($\beta_z \neq 0$, out-of-plane propagation). An example of the band structure for the oblique direction of propagation is shown in Fig. 12 for crystals with square dielectrics. Note that, due to the homogeniety, there is no photonic bandgap in the logitudinal direction. The geometry

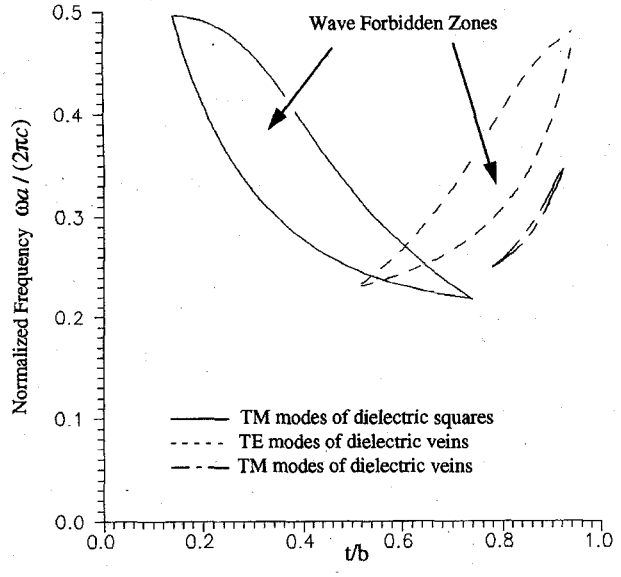

Fig. 10. Photonic bandgap map for 2-D square structures. Material dielectric constant is $\varepsilon_r = 11$.

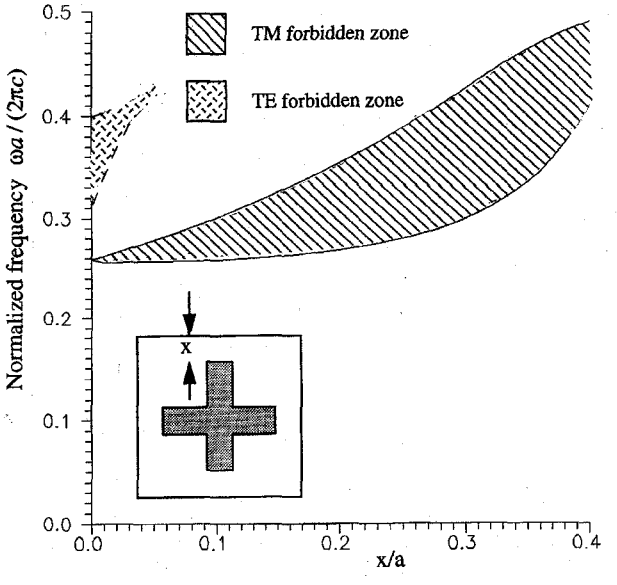

Fig. 11. Photonic bandgap for symmetric crosses versus arm length. Dielectric constant is $\varepsilon_r = 11$ and the arm width is $0.2a$.

of the structure is identical to that in Fig. 7. For out-of-plane propagation, the z-direction phase constant is assumed as $1/a$. An interesting observation is found from the comparison of these two Figures. For out-of-plane propagation, all the modes are hybrid and no bandgap is observed. It is seen from Fig. 12 that there exists transverse mode cutoff. This is no surprise since the frequency is related to the specified longitudinal phase constant. Also, if we specify the longitudinal wave number, equivalently, we are dealing with higher-order modes of parallel metal plates containing photonic crystals, where cutoff frequency exists for higher-order modes. A general observation for the modes with out-of-plane propagation is that the increase in β_z results in a percentage increase of the field intensity within the high dielectric region, and the mode curves are closer together (more crowded). Larger β_z

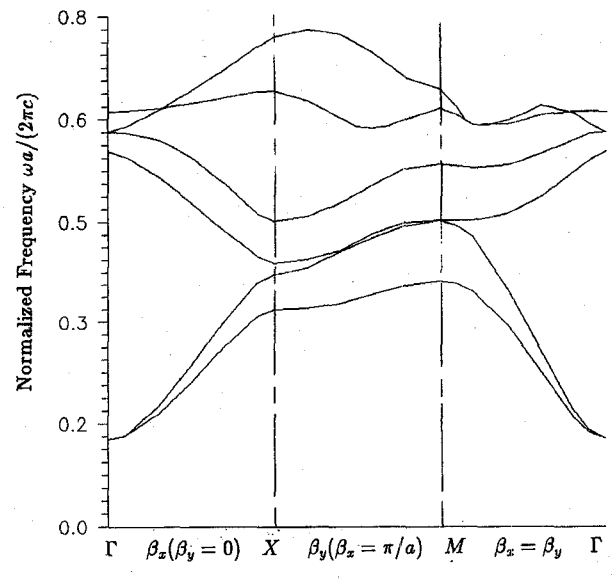

Fig. 12. The photonic band structure for the first six modes of dielectric squares $\varepsilon_r = 8.9$ surrounded by air. The square length is $0.3545a$. Out-of-plane propagation $\beta_z = 1/a$.

corresponds to less mutual coupling between implants. In the limiting case of very large β_z, we expect that all the modes in Fig. 7 will be merging together (mode curves are flat), a result of large energy density within the high dielectric region. The frequency of all the modes in this limiting case is approximately $\omega = c\beta_z/\sqrt{\varepsilon_r}$. The photonic band structure for out-of-plane modes is also of importance in the design of modeless photonic-crystal parallel-plate guides. This research is ongoing and will be presented in the near future.

IV. Conclusion

In this paper, we presented finite difference analysis for a class of 2-D photonic crystals. A numerically efficient scheme, which utilizes the quasi-band diagonal property of the characteristic matrix, was developed to reduce significantly computer time and memory for finding eigenvalues of large sparse matrices. Photonic band structures for dielectric squares, veins, and crosses as well as air crosses are investigated with emphasis on finding the photonic bandgaps, where in-plane propagation is prohibited in all directions. Such photonic bandgap materials have many engineering applications, such as for optical shields, photonic waveguides, high-Q resonators, laser emission, and protection, etc.. We concluded that with a proper filling factor, low dielectric materials with isolated high-dielectric implants show a wide TM bandgap; while low dielectric materials with connected, slim, and higher-dielectric implants show a wide TE bandgap. We also investigated the photonic band characteristics for out-of-plane propagation. We concluded that the larger the longitudinal wavenumber (β_z) is, the flatter and closer the photonic bands are. This is due to the fact that energy is most confined within the high dielectric region for large β_z, and the coupling between implants is weak. The presented finite difference analysis would also be useful for the design of modeless parallel-plate guides, photonic cavity, and waveguide. The research is ongoing.

APPENDIX

Finite difference equations for fields at a central node joined by four grids each with different dielectrics are shown in this appendix. The grids used for deriving finite difference representation of fields is shown in Fig. 13. The finite difference equations are obtained by descretizing the Helmholtz equation in the homogeneous subregions and field matching at the central node. The results for hybrid modes (H formulation of out-of-plane propagation) and TE and TM modes (in-plane propagation) are shown in the following.

a) Finite difference equations for out-of-plane propagation

$$\begin{aligned}
&\frac{2}{n(w+e)}\left(\frac{w\varepsilon_3}{s\varepsilon_2+n\varepsilon_3}+\frac{e\varepsilon_4}{n\varepsilon_4+s\varepsilon_1}\right)H_{xN}\\
&+\frac{2}{s(w+e)}\left(\frac{w\varepsilon_2}{s\varepsilon_2+n\varepsilon_3}+\frac{e\varepsilon_1}{n\varepsilon_4+s\varepsilon_1}\right)H_{xS}\\
&+\frac{2}{w(w+e)}H_{xw}+\frac{2}{e(w+e)}H_{xE}\\
&+\omega^2\mu_0\frac{n+s}{w+e}\left(\frac{w\varepsilon_2\varepsilon_3}{s\varepsilon_2+n\varepsilon_3}+\frac{e\varepsilon_1\varepsilon_4}{n\varepsilon_4+s\varepsilon_1}\right)H_{xC}\\
&-\frac{2}{(w+e)}\left(\frac{\varepsilon_1}{n\varepsilon_4+s\varepsilon_1}-\frac{\varepsilon_2}{s\varepsilon_2+n\varepsilon_3}\right)H_{yS}\\
&-\frac{2}{w+e}\left[\frac{\varepsilon_2}{s\varepsilon_2+n\varepsilon_3}\left(\frac{w}{s}+\frac{s}{w}\right)+\frac{\varepsilon_3}{s\varepsilon_2+n\varepsilon_3}\left(\frac{w}{n}+\frac{n}{w}\right)\right.\\
&\qquad\left.+\frac{\varepsilon_4}{n\varepsilon_4+s\varepsilon_1}\left(\frac{e}{n}+\frac{n}{e}\right)+\frac{\varepsilon_1}{n\varepsilon_4+s\varepsilon_1}\left(\frac{e}{s}+\frac{s}{e}\right)\right]\\
&\times H_{xC}-\frac{2}{w+e}\frac{\varepsilon_2-\varepsilon_3}{s\varepsilon_2+n\varepsilon_3}H_{yW}-\frac{2}{w+e}\frac{\varepsilon_4-\varepsilon_1}{s\varepsilon_1+n\varepsilon_4}\\
&\times H_{yE}-\frac{2}{w+e}\left(\frac{\varepsilon_3}{s\varepsilon_2+n\varepsilon_3}-\frac{\varepsilon_4}{n\varepsilon_4+s\varepsilon_1}\right)H_{yN}\\
&-\beta_z^2H_{xC}=0 \qquad (5)
\end{aligned}$$

and

$$\begin{aligned}
&\frac{2}{n(n+s)}H_{yN}+\frac{2}{s(n+s)}H_{yS}\\
&+\frac{2}{w(n+s)}\left(\frac{s\varepsilon_4}{e\varepsilon_3+w\varepsilon_4}+\frac{n\varepsilon_1}{e\varepsilon_2+w\varepsilon_1}\right)H_{yW}\\
&+\frac{2}{e(n+s)}\left(\frac{n\varepsilon_2}{e\varepsilon_2+w\varepsilon_1}+\frac{s\varepsilon_3}{e\varepsilon_3+w\varepsilon_4}\right)H_{yE}\\
&-\beta_z^2H_{yC}+\omega^2\mu_0\frac{w+e}{n+s}\left(\frac{n\varepsilon_1\varepsilon_2}{e\varepsilon_2+w\varepsilon_1}+\frac{s\varepsilon_3\varepsilon_4}{e\varepsilon_3+w\varepsilon_4}\right)H_{yC}\\
&+\frac{2}{(n+s)}\left(\frac{\varepsilon_4}{e\varepsilon_3+w\varepsilon_4}-\frac{\varepsilon_1}{e\varepsilon_2+w\varepsilon_1}\right)H_{xW}\\
&-\frac{2}{n+s}\left[\frac{\varepsilon_2}{e\varepsilon_2+w\varepsilon_1}\left(\frac{e}{n}+\frac{n}{e}\right)+\frac{\varepsilon_3}{e\varepsilon_3+w\varepsilon_4}\left(\frac{e}{s}+\frac{s}{e}\right)\right.\\
&\qquad\left.+\frac{\varepsilon_4}{e\varepsilon_3+w\varepsilon_4}\left(\frac{w}{s}+\frac{s}{w}\right)+\frac{\varepsilon_1}{e\varepsilon_2+w\varepsilon_1}\left(\frac{w}{n}+\frac{n}{w}\right)\right]\\
&\times H_{yC}+\frac{2}{n+s}\frac{\varepsilon_1-\varepsilon_2}{e\varepsilon_2+w\varepsilon_1}H_{xN}+\frac{2}{n+s}\frac{\varepsilon_3-\varepsilon_4}{e\varepsilon_3+w\varepsilon_4}H_{xS}\\
&+\frac{2}{n+s}\left(\frac{\varepsilon_2}{e\varepsilon_2+w\varepsilon_1}-\frac{\varepsilon_3}{e\varepsilon_3+w\varepsilon_4}\right)H_{xE}=0. \qquad (6)
\end{aligned}$$

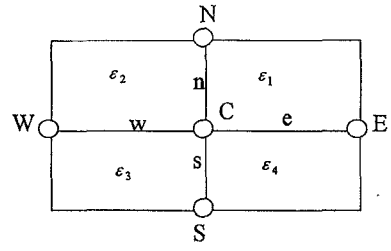

Fig. 13. A mesh with a five-point finite difference representation.

b) Finite difference equation for TM modes (in-plane propagation)

$$\begin{aligned}
&\left[\left(\frac{n}{e}+\frac{e}{n}+\frac{s}{e}+\frac{e}{s}+\frac{n}{w}+\frac{w}{n}+\frac{s}{w}+\frac{w}{s}\right)\right.\\
&\left.-\frac{k_0^2}{2}(ne\varepsilon_1+es\varepsilon_2+nw\varepsilon_3+ws\varepsilon_4)\right]E_{zC}\\
&-\frac{n+s}{e}E_{zE}-\frac{n+s}{w}E_{zW}\\
&-\frac{w+e}{n}E_{zN}-\frac{w+e}{s}E_{zS}=0. \qquad (7)
\end{aligned}$$

c) Finite difference equation for TE modes (in-plane propagation)

$$\begin{aligned}
&\left[\left(\frac{n}{e}+\frac{e}{n}\right)\frac{1}{\varepsilon_1}+\left(\frac{s}{e}+\frac{e}{s}\right)\frac{1}{\varepsilon_4}+\left(\frac{n}{w}+\frac{w}{n}\right)\frac{1}{\varepsilon_2}\right.\\
&\left.+\left(\frac{s}{w}+\frac{w}{s}\right)\frac{1}{\varepsilon_3}-\frac{k_0^2}{2}(ne+es+nw+ws)\right]H_{zC}\\
&-\left(\frac{n}{e\varepsilon_1}+\frac{s}{e\varepsilon_4}\right)H_{zE}-\left(\frac{n}{w\varepsilon_2}+\frac{s}{w\varepsilon_3}\right)H_{zW}\\
&-\left(\frac{e}{n\varepsilon_1}+\frac{w}{n\varepsilon_2}\right)H_{zN}-\left(\frac{w}{s\varepsilon_3}+\frac{e}{s\varepsilon_4}\right)H_{zS}=0. \qquad (8)
\end{aligned}$$

ACKNOWLEDGMENT

The author would like to thank N. Alexopoulos at the University of California, Los Angeles, for helpful suggestions.

REFERENCES

[1] W. E. Kock, "Metallic delay lenses," *Bell Syst. Tech. J.*, vol. 27, pp. 58–82, 1948.
[2] R. S. Elliott, *An Introduction to Guided Waves and Microwave Circuits*. New York: Prentice-Hall, 1993.
[3] J. P. Montgomery, "Scattering by an infinite periodic array of thin conductors on a dielectric sheet," *IEEE Trans. Antennas Propagat.*, vol. AP-23, pp. 70–75, Jan. 1975.
[4] R. J. Mailloux, J. F. McIlenna, and N. P. Kernweis, "Microstrip array technology," *IEEE Trans. Antennas Propagat.*, vol. AP-29, pp. 25–37, Jan. 1981.
[5] P. Sheng, Ed., *Scattering and Localization of Classical Waves in Random Media*. Singapore: World Scientific, 1990.
[6] E. Yablonovitch, "Inhibited spontaneous emission in solid-state physics and electronics," *Phys. Rev. Lett.*, vol. 58, no. 20, pp. 2059–2062, May 1987.
[7] E. Yablonovitch, T. J. Gmitter, and K. M. Leung, "Photonic band structures: The face-centered-cubic case employing nonspherical atoms," *Phys. Rev. Lett.*, vol. 67, no. 17, pp. 2295–2298, Oct. 1991.
[8] R. D. Meade, K. D. Brommer, A. M. Rappe, and J. D. Joannopoulous, "Existence of a photonic band gap in two dimensions," *Appl. Phys. Lett.*, vol. 61–64, no. 27, pp. 495–497, July 1992.
[9] J. D. Joannoploulos, R. D. Meade, and J. N. Winn, *Photonic Crystals*. Princeton, NJ: Princeton Univ. Press, 1995.

[10] K. Bierwirth, N. Schulz, and F. Arndt, "Finite-difference analysis of rectangular dielectric waveguide structures," *IEEE Trans. Microwave Theory Tech.*, vol. 34, pp. 94–103, Nov. 1986.
[11] B. S. Garbow, J. M. Boyle, J. J. Dougarra, and C. B. Moler, "Matrix eigensystem routines-EISPACK guide extension," in *Lecture Notes in Computer Science*. Heidelberg: Springer-Verlag, 1977, vol. 51.
[12] H. Y. Yang, J. A. Castaneda, and N. G. Alexopoulos, "An integral equation analysis of an infinite array of rectangular dielectric waveguides," *IEEE Trans. Microwave Theory Tech.*, vol. 38, pp. 873–880, July 1990.
[13] P. J. B. Clarricoats and B. C. Taylor, "Evanescent and propagating modes of dielectric-loaded circular waveguids," *Proc. IEE,* vol. 111, pp. 1951–1956, Dec. 1964.

Hung Yu David Yang (S'87–M'88–SM'93) received the B.S. degree in electrical engineering from the National Taiwan University, Taipei, and the M.S. and Ph.D. degrees in electrical engineering from the University of California at Los Angeles in 1982, 1985, and 1988, respectively.

During 1988–1992, he was with Phraxos R&D Inc. as a research engineer. where he was involved in the development of computer codes for frequency-selective surfaces, scattering from antennas, design of microstrip antenna arrays, and antennas on nonreciprocal materials. Since August 1992, he has been an assistant professor with the Department of Electrical Engineering and Computer Science, University of Illinois at Chicago. He has published more than 60 journal and conference papers. His recent research interest has been on the development of new computational methods for radiation and scattering from artificial periodic materials; vector integral-equation method and frequency-domain finite difference method for photonic band-gap structures and advanced materials; wave interaction with bianisotropic media; printed circuits, and antennas on gyrotropic media.

Dr. Yang has served as an Associate Editor of the IEEE TRANSACTIONS ON ANTENNAS AND PROPAGATION since 1995 and a technical program member of the IEEE Microwave Symposium since 1994.